NASA Technical Memorandum 109026
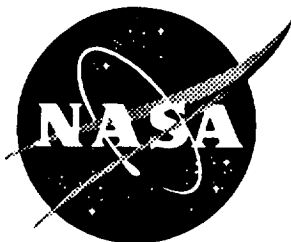
Prediction of Stress-Strain Response of SCS-6/Timetal-21S Subjected to a Hypersonic Flight Profile

M. Mirdamadi
Analytical Services and Materials, Inc., Hampton, Virginia

W. S. Johnson
Langley Research Center, Hampton, Virginia

February 1994

National Aeronautics and
Space Administration
Langley Research Center
Hampton, Virginia 23681-0001

Prediction of Stress-Strain Response of SCS-6/Timetal-21S Subjected to a Hypersonic Flight Profile

M. Mirdamadi[1] and W. S. Johnson[2]

Thermomechanical response of a cross-ply SCS-6/Timetal-21S composite subjected to a generic hypersonic flight profile with the temperature ranging from -130°C to 816°C was evaluated experimentally and analytically. A two dimensional micromechanical analysis, VISCOPLY, was used to predict the stress-strain response of the laminate and of the constituents in each ply during thermomechanical loading conditions. In the analysis, the fiber was modeled as elastic with transverse orthotropic and temperature dependent properties and the matrix was modeled using a thermo-viscoplastic constitutive relation. The fiber transverse modulus was reduced in the analysis to simulate fiber-matrix interface failure. Reasonable agreement was found between measured and predicted laminate stress-strain response when fiber-matrix debonding was modeled.

INTRODUCTION

Titanium matrix composites (TMC) reinforced with continuous silicon fibers are being considered as structural materials for elevated temperature applications in future generation hypersonic vehicles. In such applications, TMC components will be subjected to complex flight profiles consisting of fatigue loading cycles, creep-fatigue loading cycles, and thermomechanical fatigue (TMF) loading at various elevated temperatures. Due to the large differences in the thermal and mechanical properties of the fiber and the matrix, significant thermal residual stresses are developed in the composite. The resulting stress coupled with applied thermal and mechanical loading, can lead to a complex state of stress in these composites. In order to develop life prediction methodologies for TMC, one must be able to predict the stresses and strains that occur in the constituents of the composite during the complicated TMF loading profiles. Therefore, a micromechanical based analyses, that can account for viscoplastic behavior of the both fiber and matrix, are very attractive and helpful in establishing a framework for a life prediction methodology.

In recent studies [1,2], such a micromechanics based analysis was used to predict the stress-strain response of a unidirectional SCS-6/Ti-15-3 composite subjected to the in-phase and out-of-phase TMF loading and a cross-ply SCS-6/Ti-15-3 composite subjected to a TMF flight profile. Good agreement between experimental results and predictions was found. The analysis also described the complex global behavior of the composite and the local behavior of the constituents subjected to TMF loading conditions.

[1]Research Scientist, Analytical Services and Materials Inc., Hampton, VA 23666.
[2]Senior Research Scientist , NASA Langley Research Center, Hampton, VA 23681.

The objective of this research is to experimentally determine the global stress-strain response of a $[0/90]_{2s}$ SCS-6/Timetal-21S composite subjected to a generic hypersonic flight profile with the temperature ranging from -130°C to 816°C and to analytically predict the measured global laminate stress-strain response. The analysis also included fiber-matrix interface failure.

ANALYTICAL METHOD - VISCOPLY

A two dimensional micromechanical model, and the associated computer code (VISCOPLY), was used to predict the stress-strain response of the composite. The VISCOPLY code, developed by Bahei-El-Din, uses the vanishing fiber diameter (VFD) model [3] to calculate the orthotropic properties of a ply. The ply properties are then used in a laminated plate theory [4] to predict the overall laminate response. Both the fiber and the matrix can be described as a thermo-viscoplastic material.

The viscoplastic constitutive model implemented in the VISCOPLY program was developed by Bahei-El-Din, Shah and Dvorak [5] for high temperature, isothermal and nonisothermal, applications and is based on the viscoplastic theory of Eisenberg and Yen [6]. This constitutive viscoplastic model assumes the existence of an equilibrium stress-strain response which corresponds to the theoretical lower bound of the dynamic response. In addition, this constitutive viscoplastic model assumes that the elastic response is rate-independent and that inelastic rate-dependent deformation takes place if the current stress state is greater than the equilibrium stress. The inelastic strain rate is described using a power law function of overstress [7] which is defined as the difference between the current stress and the equilibrium stress. Under tensile loading condition, this inelastic strain rate can be written as;

$$\dot{\varepsilon}_{in} = k(\sigma - \sigma^*)^p \qquad (1)$$

where σ is the current stress, σ^* is the equilibrium stress, and k and p are the material constants. The material constants, k and p, are needed to describe the viscoplastic response for a given temperature. When isotropic hardening and thermal recovery effects are not significant, these parameters can be determined from two monotonic uniaxial tests. Determination of the viscoplastic material constants is presented in the Experimental Techniques section of this paper.

Complex combinations of thermal and mechanical loads can be readily modeled using the VISCOPLY program. Sequential jobs can be run to vary the order and rate of load and temperature. Fiber and matrix average stresses and strains and the overall composite response under thermomechanical loading conditions are calculated. Due to the assumptions made in the of VFD model, local micromechanical effects such as the lateral constraint of the matrix due to the presence of the fibers and stress concentrations in the

fibers and matrix are not accounted for in the VISCOPLY program. Nevertheless, the VISCOPLY program has been used to predict the global thermomechanical response within 10% of the experimental results in similar TMC [1,2].

Fiber-matrix interface failure in TMC occurs early under applied load and causes significant changes in the global stress-strain response [8] and must be accounted for in any analysis. Experimental data [8] showed that the failure of the fiber-matrix interface corresponds to a distinct knee in the stress-strain curve. Previous work [2] on $[0/90]_{2s}$ SCS-6/Ti-15-3 composites showed that the fiber-matrix interface failure can be simulated by reducing the fiber transverse modulus, E_t^f, in the 90° plies at the stress level corresponding to the observed knee in the stress-strain curve of the $[0/90]_{2s}$ laminate at room temperature. In elevated temperature fatigue tests, thermal residual stresses were relieved and no knee was apparent in the stress-strain response. It was therefore assumed that, for temperatures above 400°C, the fiber-matrix interfacial failure occurred upon loading and the fiber transverse modulus in the 90° plies was reduced at the start of loading [2]. It was found [2] that by multiplying the fiber transverse modulus of the 90° plies by 0.1 ($E_t^f / E_a^f = 0.1$, where E_a^f is the fiber axial modulus) gave the best overall fit to the experimental data as shown in the Figure 1. This factor will be used in all predictions of the $[0/90]_{2s}$ SCS-6/Timetal-21S composite to simulate fiber-matrix interface failure.

MATERIAL AND TEST SPECIMENS

The material used in this study was SCS-6/Timetal-21S which was fabricated into a $[0/90]_{2s}$ laminate by hot isostatic pressing (HIPing) Ti-15Mo-3Nb-3Al-0.2Si foil between tapes of unidirectional SCS-6 silicon-carbide fibers having a diameter of 0.14 mm. The fibers were held in place with Ti-Nb crossweave wires. An average volume fraction of 0.365 was measured for this laminate.

Rectangular specimens having a length of 152 mm, width of 12.7 mm and thickness of 1.69 mm, were machined using a diamond wheel saw. Brass tabs (10 mm x 30 mm x 1 mm) were placed between the end of the specimen and the grips to avoid specimen failure in the grips. Prior to testing, each specimen was heat treated (aged) at 621°C for eight hours in vacuum to stabilize matrix material.

EXPERIMENTAL TECHNIQUES

All the experiments were conducted using a 100-kN closed-loop servohydraulic test frame equipped with water-cooled hydraulic grips. In addition, the test frame was equipped with a load profiler capable of running predetermined strain or load profiles. The test specimen was heated using a 5-kW induction generator with three independent adjustable coils such as developed by Ellis and co-workers [9]. The induction generator was controlled by a temperature profiler capable of running predetermined temperature

3

profiles. K-type thermocouples were used to monitor and control the temperature along a 50-mm gage length section in the center of the specimen. In addition, an infrared thermovision camera was used to insure that a uniform temperature distribution was achieved along the gage section of the specimen. Axial strains were measured on the edge of the specimen using a high temperature, quartz rod water-cooled extensometer with a 25-mm gage length. An eight channel analog-digital PC based data acquisition system was used to record and store the test data in terms of stress, strain, and temperature as a function of time.

Isothermal - Matrix Characterization

The matrix material constants needed for input by the VISCOPLY program are given in Table 1. These material constants include coefficient of thermal expansion (CTE), elastic modulus (E), yield stress (Y), equilibrium stress-strain curve parameters (A and n), and viscoplastic parameters (k and p), for a given temperature. CTE was determined from the results of a load-controlled experiment. The CTE test specimen, under zero load, was subjected to temperature increments ranging from $-130^{\circ}C$ to $816^{\circ}C$. At each increment, the temperature was held constant (about 1 minute) to allow for stabilization. The temperatures and the corresponding thermal strains were fitted to a third degree polynomial using method of least squares as shown in Figure 2. The resulting polynomial function was differentiated with respect to temperature to determine CTE as a function of temperature. The elastic modulus (E) and the yield stress (Y) were determined from the linear portion and onset of nonlinearity of the stress-strain curve at each temperature of interest, respectively.

To define the equilibrium stress-strain curve, strain-controlled tests were conducted with 5-minute hold-periods imposed at predetermined strain levels to allow stress relaxation to occur. The strain-rate during loading was 1×10^{-4} mm/mm per second. Duration of hold-period and strain-rate were chosen based on previous work on similar TMC [2]. These tests were similar in approach to those outlined by Eisenberg and Yen [6] and are schematically shown in Figure 3. At each temperature, a minimum of five strain levels were selected to construct the equilibrium stress-strain curve. The equilibrium curve was then approximated by fitting to a power law equation,

$$\sigma^* = A \, (\varepsilon_{in})^n \tag{2}$$

using the method of least squares, to the observed values of the stress at the ends of hold periods and corresponding inelastic strain (ε_{in}) determined from the following equation,

$$\varepsilon_{in} = \varepsilon_t - \sigma^*/E \tag{3}$$

where ε_t is the known predetermined total strain value. The curve fitting parameters A and n in Eq (2) are given in Table 1

The load-controlled monotonic tests used to determine the rate-dependent deformation were conducted at a constant stress-rate of 2.56 MPa per second. The stress-rate was chosen based on previous work on similar TMC [2]. Given the equilibrium curve, the overstress can be determined as illustrated in Figure 4a. To facilitate the numerical manipulation, the stress (σ) and corresponding inelastic strain values (ε_{in}) determined from the load-controlled test were also fit to a power law equation

$$\sigma = C \, (\varepsilon_{in})^m \tag{4}$$

using the method of least squares. The strain value (ε_{in}) was calculated similar to Equation (3) except σ^* is replaced by σ, the current stress. C and m are curve fitting parameters. The resulting equation was differentiated with respect to time as follows,

$$\dot{\sigma} = \frac{d\sigma}{dt} = \frac{d\sigma}{d\varepsilon_{in}} \cdot \frac{d\varepsilon_{in}}{dt} = \frac{d\sigma}{d\varepsilon_{in}} \dot{\varepsilon}_{in} \tag{5}$$

By substituting Equation (4) into Equation (5) and rearranging, the inelastic strain rate can be written as,

$$\dot{\varepsilon}_{in} = \frac{\dot{\sigma}}{Cm}(\varepsilon_{in})^{1-m} \tag{6}$$

Knowing the stress-rate ($\dot{\sigma}$ = 2.56 MPa/Sec) and the curve fitting parameters C and m, from Equation (4), the inelastic strain rate ($\dot{\varepsilon}_{in}$) can be calculated from Equation (6) for a given inelastic strain. The viscoplastic material constants (k and p) were then determined by fitting a power law equation (Equation (1) to the inelastic strain rate (Equation (6)) and overstress(σ - σ^*), determined from Equations (2) and (4), using method of least squares technique as illustrated in Figure 4b. The material constants needed for input by the VISCOPLY program are summarized in Table 1, the material parameters constants C and m are not directly needed for input by the VISCOPLY program so are subsequently not listed in Table 1.

TMF test setup

A TMF test capability developed previously [2] was modified to conduct a generic hypersonic flight profiles such as shown in Figures 5a and 5b. As indicated in the figures the flight profile consisted of Mission I and Mission II. The letters shown in Figures 5a and 5b will be used later for comparison with the stress-strain results. The entire TMF flight profile shown in Figure 5a is applied 24 times followed by the TMF flight profile shown in Figure 5b once. This sequence is repeated until the failure of the test specimen. The temperature profiles shown in Figures 5a and 5b are the same with a maximum and

minimum applied temperature of 815°C and -130°C, respectively. The heating and cooling rates of the temperature profile are 2.8°C/sec and 1.4°C/sec, respectively. The loading profiles in Figures 5a and 5b have slight differences. In Figure 5a, the maximum applied stress in the loading profile is 336 MPa, while the maximum applied stress in Figure 5b is 420 MPa. In addition, Figure 5b contains the segment of the loading profile designated as d-e-f which is in-phase with the applied temperature. The mechanical fatigue cycles are applied at a frequency of 1 Hz. In all the TMF test experiments, the test specimen was subjected to thermal loading history prior to mechanical loading. This step was necessary to assure precise synchronization between the applied temperature and the mechanical load signals.

Details of the TMF test setup are given in [2]. Briefly, the TMF test setup consists of a 100-kN, closed-loop, servohydraulic test frame equipped with water-cooled hydraulic grips, a load profiler, a 5-kW induction generator controlled by a temperature profiler, and a nitrogen supply tank. The temperature profiler was interfaced with the load profiler to initiate the temperature spectrum at any desired segment in the load profile. This assures precise synchronization between mechanical and thermal loading profiles. In addition, the temperature profiler was modified so that the cryogenic temperatures (as low as -130°C) could be controlled. The nitrogen supply tank was modified to supply gaseous or liquid nitrogen, depending on the required cooling rate. The flow of gaseous and liquid nitrogen was controlled by the temperature profiler during the cool down portion of the temperature profile. The combined use of gaseous and liquid nitrogen with induction heating was necessary to maintain the desired cooling rate of 1.4°C/sec and to reached the minimum temperature of -130°C.

RESULTS AND DISCUSSIONS

In this section, the constituent properties are presented, the isothermal neat Timetal-21S matrix behavior is analyzed using VISCOPLY and compared with observed experimental behavior. Experimental data and VISCOPLY predictions of the stress-strain response of a $[0/90]_{2s}$ SCS-6/Timetal-21S composite subjected to a generic hypersonic flight profile are presented and compared.

Constituent Properties

The temperature dependent thermal and mechanical properties of the fiber used in this study are shown in Table 2 [11]. In the analysis, the fiber was assumed to remain elastic with transverse orthotropic properties. The temperature-dependent and rate-dependent material properties of the neat Timetal-21S matrix were determined from tests of the matrix material conducted at room temperature and elevated temperatures of 316°C, 427°C, 482°C, 566°C, 621°C, 650°C, 704°C, and 760°C and are given in Table 1. Values from Table 1 will be used for all predictions shown here-in.

6

Timetal-21S Matrix Behavior

To verify the accuracy of the material constants for the Timetal-21S matrix (Table 1), the analytical predictions were compared to experimental data from the literature tests [12] and the present study of the Timetal-21-S matrix that were conducted under strain control at different temperatures.

The cyclic stress-strain response of the neat Timetal-21S at $650^{\circ}C$ with a strain rate of 83.3×10^{-6} /sec and at $760^{\circ}C$ with the strain rates of 83.3×10^{-6} /sec and 833.3×10^{-6} /sec are shown in Figures 6, 7, and 8, respectively [5]. The tests were conducted at an applied total strain range of $\pm 1\%$. As seen in the figures VISCOPLY accurately predicted the cyclic stress-strain response of the Timetal-21S using only the material constants (determined under tensile loading conditions) shown in Table 1.

The time-dependent response of the neat Timetal-21S at $760^{\circ}C$, determined from the cyclic stress-relaxation test, is shown in Figure 9. The strain rate during loading was 1×10^{-4} /sec with a 300 second hold-time applied at the pre-determined strain levels of 0.0025, 0.005, 0.0075, 0.01, 0.015, and 0.02. Also shown in the figure is the VISCOPLY prediction. As seen in the figure VISCOPLY accurately predicted the maximum stress and the initial portion of the stress relaxation response. However, the experimentally observed stresses at the end of the hold periods were lower than the VISCOPLY prediction (see Figure 10) which may be due to the isotropic hardening and thermal recovery effects which are not accounted for in the VISCOPLY program.

Laminate Behavior

A thermal response test on the cross-ply laminate was conducted by applying only the thermal history of the flight profile shown in Figure 5. The measured thermal strains and the VISCOPLY predictions are shown in Figure 10. As seen in the figure, thermal strain of the laminate was accurately predicted by the VISCOPLY program and the constituents material properties shown in Tables 1 and 2.

The test specimen was then subjected to the full thermal and mechanical flight profiles shown in Figure 5a and Figure 5b. The horizontal segments of the experimental data indicate an increase in strain due to temperature change while the mechanical load was held constant. The experimental data of the 1st, 5th, and 25th flights are shown in Figures 11 through 13. For clarity, different symbols have been used for Mission I and Mission II. Also shown in the figures are the VISCOPLY predictions with the simulated failure of the fiber-matrix interface of the 90°plies. The letters placed at various locations on the stress-strain response can be referenced back to Figure 5 to find the associated segment on the flight profile. The predictions of the cyclic load, at point K and S, appear broad because the temperature was changing. As seen in Figure 11, VISCOPLY reasonably predicted the observed experimental stress-strain response of the 1st flight. However, a larger permanent strain was observed experimentally (as noted in the figure)

7

than was predicted using VISCOPLY, indicating that other types of damage (such as local plasticity) are occurring which are not accounted for in the VISCOPLY analysis. The experimental stress-strain response stabilized rather quickly (after 2 flights). However, VISCOPLY predictions did not stabilize until the fifth flights. The experimental stress-strain response and of the VISCOPLY prediction of the 5th flight are shown in Figure 12. In the VISCOPLY analysis, the permanent strain observed experimentally during the 5th flight was matched with the strain at start of the analysis. As shown in the figure, the VISCOPLY predicted the stabilized flight stress-strain response reasonably. The experimental stress-strain response of the 25th flight (using profile shown in Figure 5b) is shown in Figure 13. Also shown in the figure is the VISCOPLY prediction. As before, the observed permanent strain as a result of flight cycling was incorporated into the VISCOPLY prediction. As seen in the figure, VISCOPLY accurately predicted the observed experimental results.

A second TMF flight profile test was conducted using a portion of the flight profile (portion A-N in Figure 5(a) and a-h in Figure 5(b)) with minimum and maximum applied temperatures of $21^{\circ}C$ and $816^{\circ}C$, respectively. The experimental stress-strain response of the 1st, 5th and 25th flights and the VISCOPLY predictions are shown in Figures 14-16, respectively. As before, the letters placed at various locations on the stress-strain response can be referenced back to Figure 5 to find the associated segment on the flight profile. As seen in Figure 14, VISCOPLY predicted the observed experimental stress-strain response reasonably. However, the predicted permanent strain during the 1st flight was smaller than the experimental observation. As mentioned earlier other types of damage mechanisms (such as local plasticity) are taking place which are not accounted for in the VISCOPLY program. The experimental stress-strain response and of the VISCOPLY prediction of the 5th flight are shown in Figure 15. As mentioned before, the experimentally observed permanent strain was incorporated into the VISCOPLY prediction. As seen in the figure, VISCOPLY accurately predicted the stabilized stress-strain response of the composite subjected to the Mission I of the flight profile. Figure 16 shows the experimental stress-strain response of the composite after 25 flights (using Mission I profile shown in Figure 5b). Also shown in the figure is the VISCOPLY prediction. As before, the observed permanent strain as a result of flight cycling was incorporated into the VISCOPLY prediction. As seen in the figure, VISCOPLY accurately predicted the observed experimental results.

A third TMF test was conducted using a portion of the Mission I of the flight profile shown in Figure 5(b) segments "b" through "h". The experimental stress-strain response and the VISCOPLY predictions of the first five cycles are shown in Figure 17. As seen in the figure, the experimental stress-strain response stabilized quickly (after cycle 2) while the VISCOPLY prediction did not stabilize until cycle 4. The VISCOPLY predictions are in excellent agreement with the experimental stress-strain response. The variation of 0° fiber stress with time for five cycles as predicted by VISCOPLY is shown in Figure 18. As seen in the figure, the maximum fiber stress increases with each subsequent cycle until cycle five. The increase in fiber stress is due to stress relaxation in

the matrix and subsequent load transferal to the fibers as predicted by the VISCOPLY program.

SUMMARY

Viscoplastic material response of the neat Timetal-21S matrix was characterized over the temperature range of 21°C to 760°C and the material constants needed for input into VISCOPLY were determined. VISCOPLY was used to analyze the rate-dependent behavior of the neat Timetal-21S matrix. A micromechanics analysis, VISCOPLY, was used to analyze the stress-strain response of the $[0/90]_{2s}$ SCS-6/Timetal-21S composite subjected to the flight profiles. The following conclusions were made:

o   VISCOPLY reasonably predicted the cyclic stress-strain response of the neat Timetal-21S matrix at the temperatures of 650°C and 760°C.

o   In TMC composite fiber-matrix interface failure must be modeled for accurate predictions. Fiber-matrix interface failures were modeled in the VISCOPLY program by multiplying the transverse modulus of the fiber in the 90°plies by 0.1.

o   The mechanical response of the composite is rate-dependent at elevated temperatures. VISCOPLY analysis can accurately predict such dependence.

o   VISCOPLY accurately predicted the composite stress-strain response for a generic hypersonic flight profile.

ACKNOWLEDGMENT

REFERENCES

[1] Mirdamadi M., and Johnson W. S., "Stress-Strain Analysis of a $[0/90]_{2s}$ Titanium Matrix Laminate Subjected to a Generic Hypersonic Flight Profile," NASA TM-107584, NASA Langley Research Center, March 1992.

[2] Mirdamadi, M., Johnson, W. S., Bahei-El-Din, Y.A., and Castelli, M. G., "Analysis of Thermomechanical Fatigue of Unidirectional Titanium Metal Matrix Composite," *Composite Materials: Fatigue and Fracture, Fourth Volume, ASTM STP 1156*, W. W. Stinchcomb and N. E. Ashbaugh Eds., American Society for Testing and Materials, Philadelphia, 1993, pp. 591-607

[3] Dvorak, G. J. and Bahei-El-Din, Y. A., "Plasticity Analysis of Fibrous Composites," *Journal of Applied Mechanics*, Vol. 49, 1982, pp. 327-335.

[4] Bahei-El-din, Y. A., "Plasticity Analysis of Fibrous Composite Laminates Under Thermomechanical Loads," *Thermal and Mechanical Behavior of Ceramic and Metal Composites, ASTM STP 1080*, J. M. Kennedy, N. H. Moeller, and W. S. Johnson, eds., American Society for Testing and Materials, Philadelphia 1990, pp. 20-39.

[5] Bahei-El-Din, Y. A., Shah, R. S., and Dvorak, G. J., "Numerical Analysis of the Rate-Dependent Behavior of High Temperature Fibrous Composites" AMD, Vol. 118: Mechanics of Composites at Elevated temperatures, S. N. Singhal, W. F. Jones, C. T. Herakovich, and T. Cruse, Eds., 1991, pp. 67-78.

[6] Eisenberg, M. A. and Yen, C. F., "A Theory of Multiaxial Anisotropic Viscoplasticity," *ASME Journal of Applied Mechanics*, Vol. 48, 1981, pp. 276-284.

[7] Malvern, L. E., "The Propagation of Longitudinal Waves of Plastic Deformation in a Bar of Material Exhibiting a Strain-Rate Effect," *ASME Journal of Applied Mechanics*, Vol. 18, 1951, pp. 203-208.

[8] Johnson, W. S., Lubowinski, S. L., and Highsmith, A. L., "Mechanical Characterization of Unnotched SCS_6/Ti-15-3 Metal Matrix Composites at Room Temperature," *Thermal and Mechanical Behavior of Metal Matrix and Ceramic Matrix Composites, ASTM STP 1080*, J. M. Kennedy, H. H. Moeller, and W. S. Johnson Eds., American Society for Testing and Materials, Philadelphia, 1990, pp. 193-218.

[9] Ellis, J.R. and P.A. Bartolotta, "Adjustable Work Coil Fixture for Facilitating the Use of Induction Heating in Mechanical Testing," NASA TM-102461, NASA Lewis Research Center, June 1989.

[10] Khobaib, M. and Ashbaugh, N. E., "Tensile, Creep, and LCF Behavior of Fiberless Timetal 21S Alloy," Fatigue 93, Vol. II, May, 1993, pp. 909-914.

[11] Bigelow, C. A., "Thermal Residual Stresses in Silicon-Carbide/Titanium [0/90] Laminate," NASA TM 107649, NASA Langley Research Center, July, 1992.

Table 1. Thermoviscoplastic Material Constants of Timetal-21s Matrix Material for Use in VISCOPLY[1]

Temp (°C)	Coefficient of Thermal Expansion, CTE (mm/mm)/°C	Elastic Modulus, E (GPa)	Yield Stress, Y (MPa)	Equilibrium Stress-Strain Curve Constants		Viscoplastic Material Constants	
				A (MPa)	n	k (MPa)$^{-p}$s^{-1}	p
21	8.62E-06	116	910	1042	0.0138	2.10E-21	8.59
150	8.72E-06	116	910	1042	0.0138	2.10E-21	8.59
316	9.23E-06	104	650	865	0.0350	2.92E-16	6.52
427	9.87E-06	103	550	848	0.0350	1.66E-14	5.62
482	10.3E-06	96	472	663	0.0320	5.38E-18	6.35
566	11.1E-06	86	275	518	0.117	6.07E-18	5.52
621	11.5E-06	80	87	268	0.135	6.05E-13	3.58
650	11.8E-06	64	44	110	0.086	1.76E-13	3.97
704	12.0E-06	53	20	79	0.14	2.66E-10	3.04
760	12.5E-05	50	8	28	0.132	1.00E-08	2.40

1- aged at 621°C in vacuum for 8 hours

Table 2. Temperature-Dependent Properties of the SCS-6 Fiber [11].

Temperature	Coefficient of Thermal Expansion CTE x 10^6	Elastic modulus	Poisson's ratio
(°C)	(mm/mm)/°C	(GPa)	
21	3.56	393	0.25
93	3.56	390	0.25
204.	3.62	386	0.25
316	3.73	382	0.25
427	3.91	378	0.25
538	4.1	374	0.25
650	4.3	370	0.25
760	4.41	365	0.25
871	4.57	361	0.25
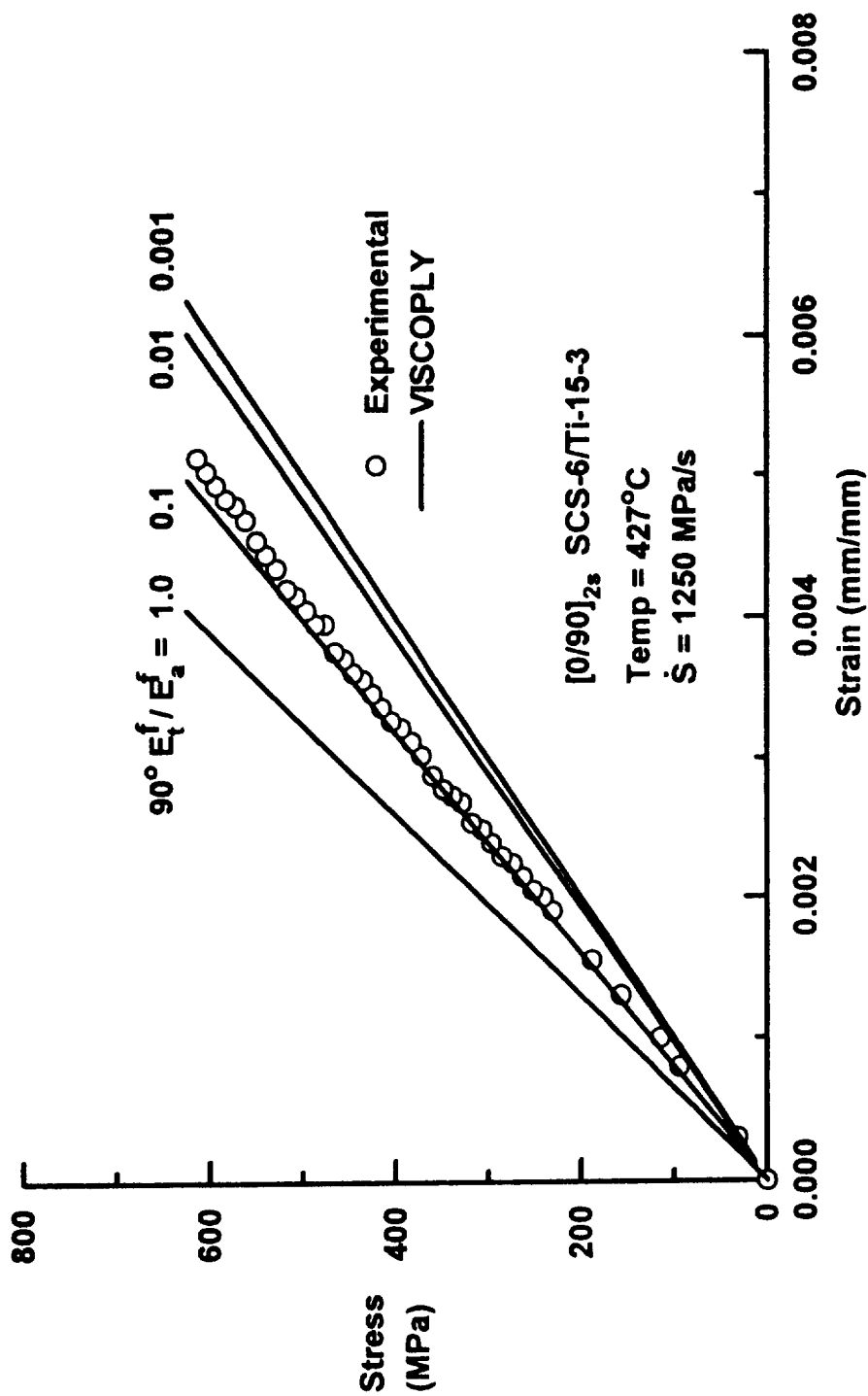
Figure 1. Effect of reducing fiber transverse modulus on VISCOPLY prediction [2].

13

$\varepsilon_{th} = -0.0002671 + 9.038\text{E-}6\ T - 1.441\text{E-}9\ T^2 + 3.649\text{E-}12\ T^3$
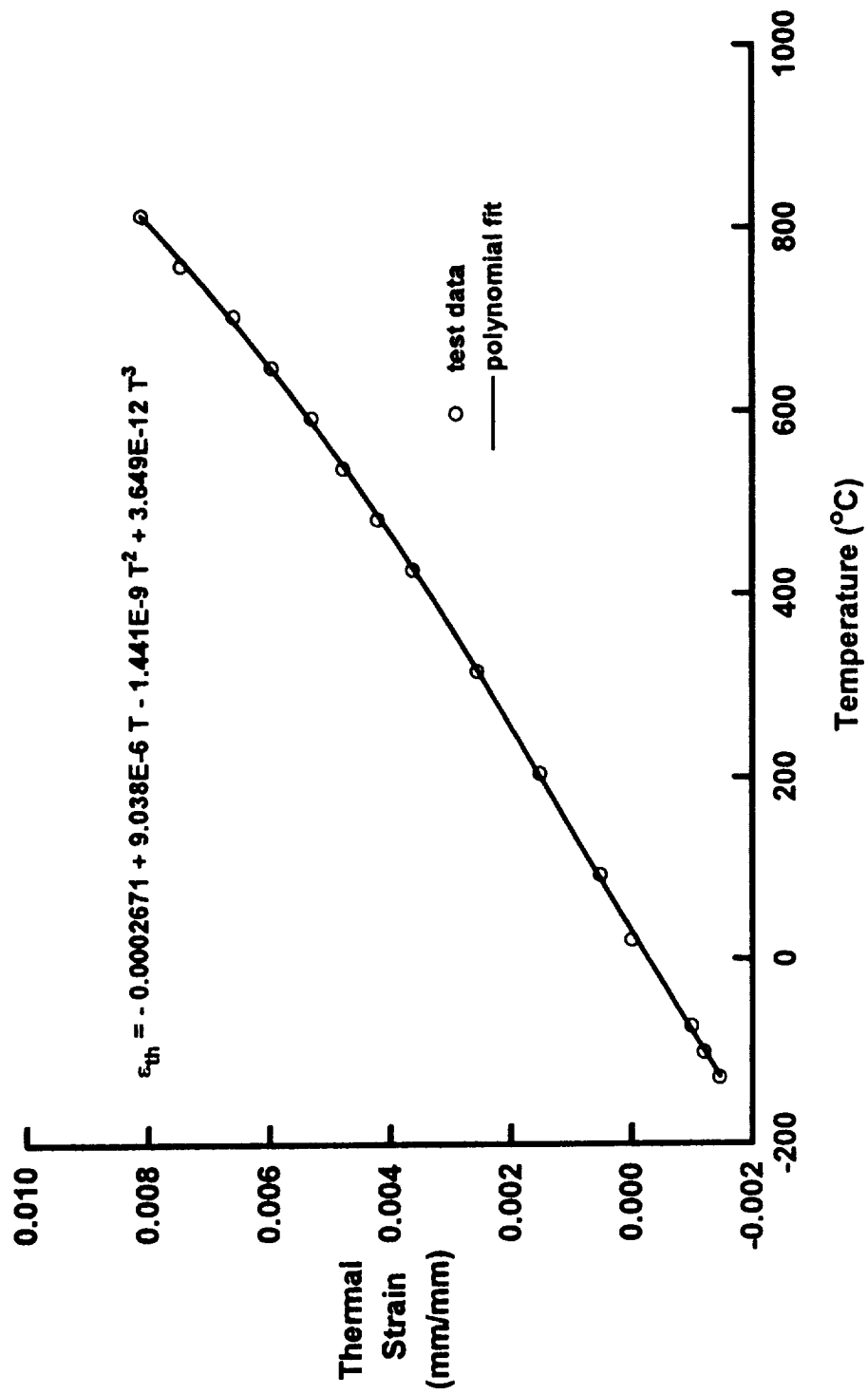
Figure 2.   Unconstrained thermal strain of neat Timetal-21S as a function of temperature.

14
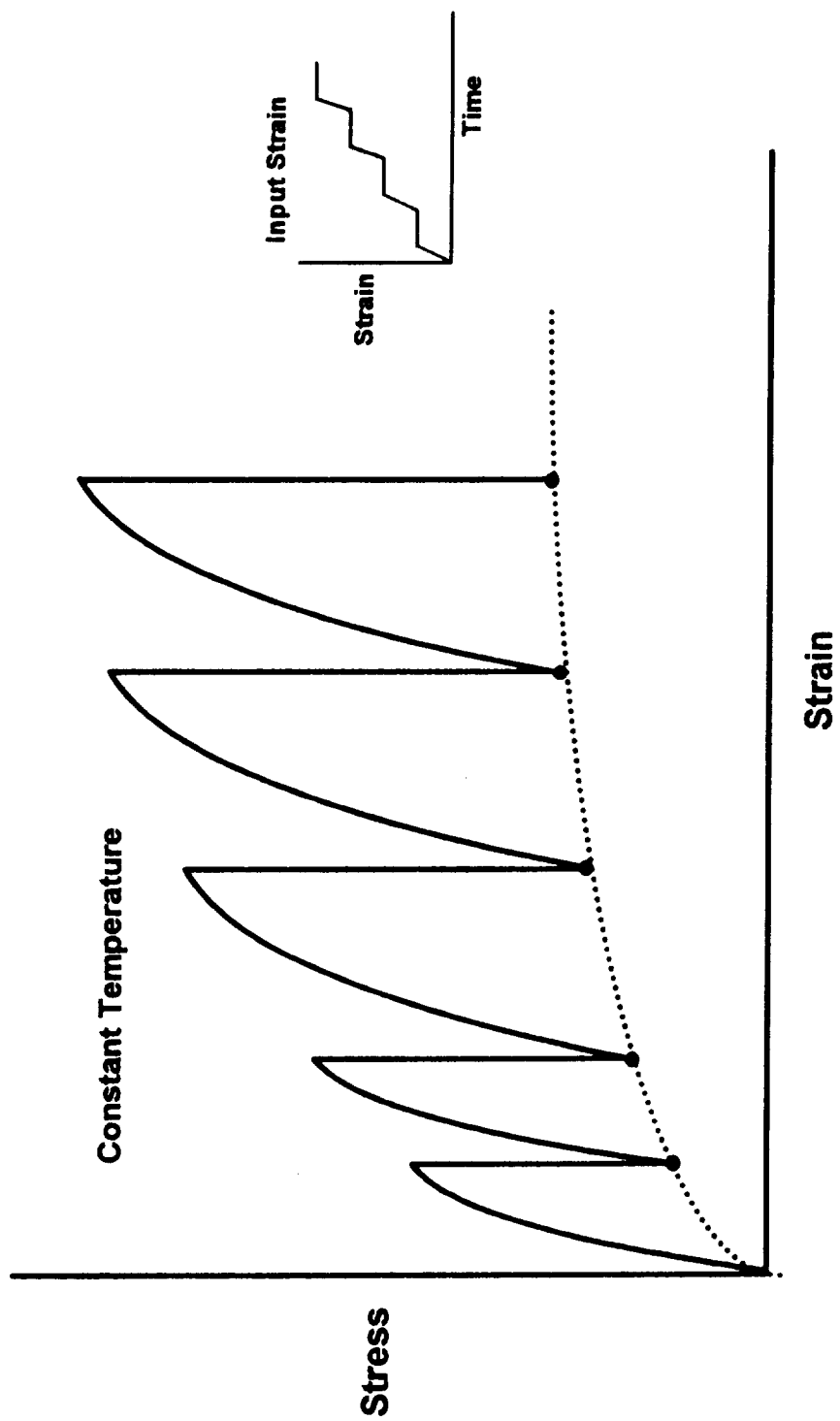
Figure 3. Determination of the equilibrium stress-strain curve.
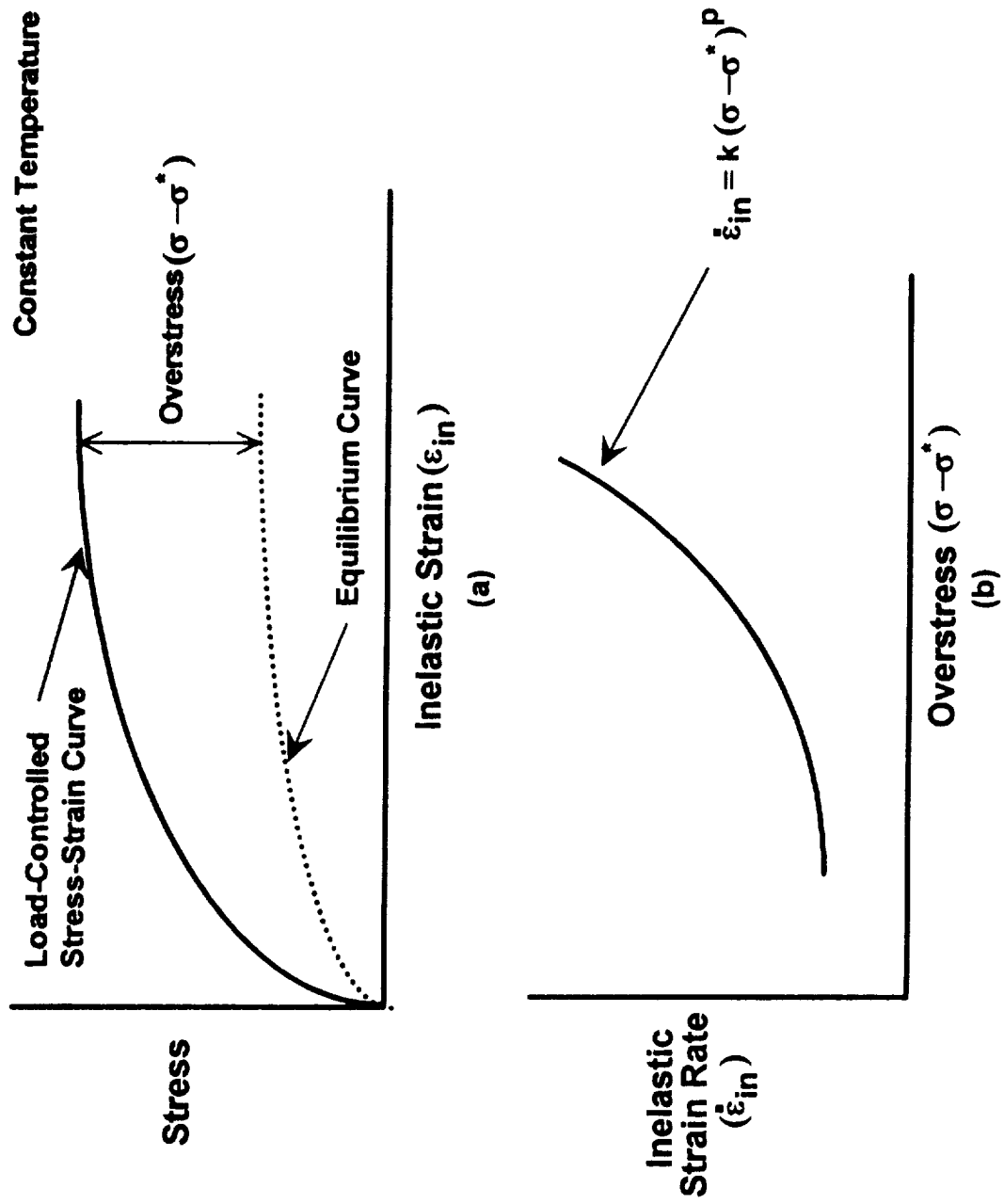
Figure 4. Determination of the viscoplastic material parametrs, k and p.
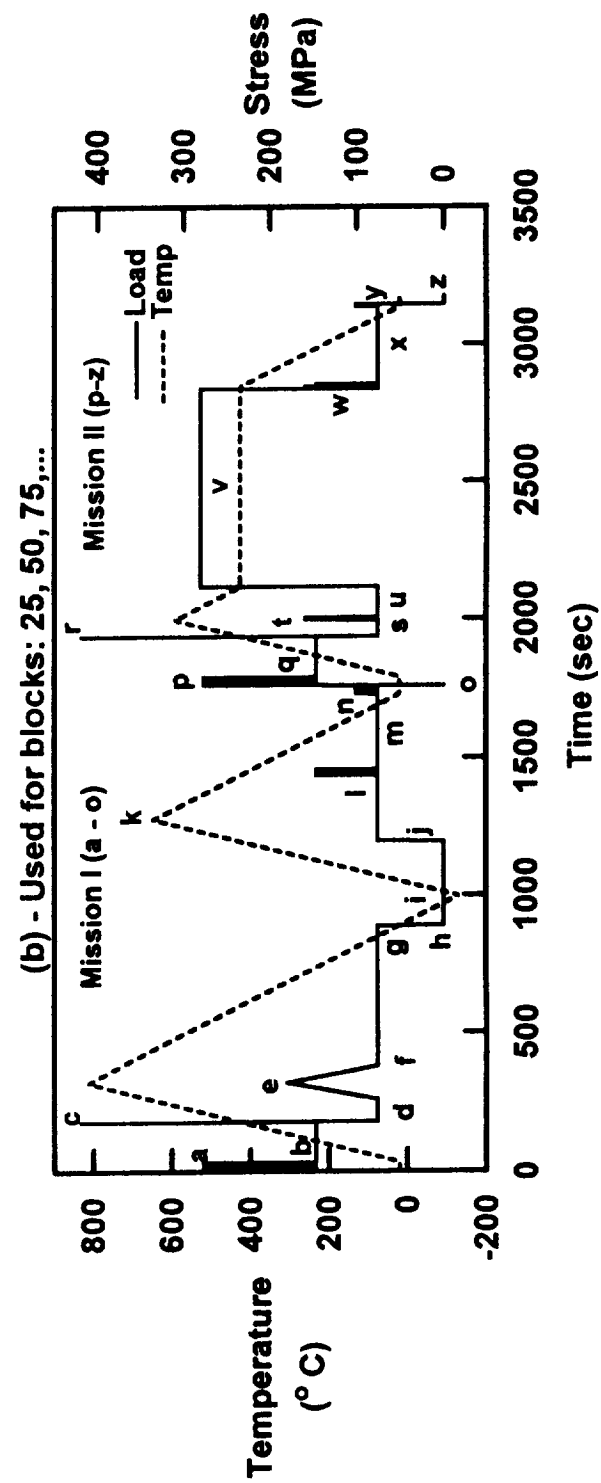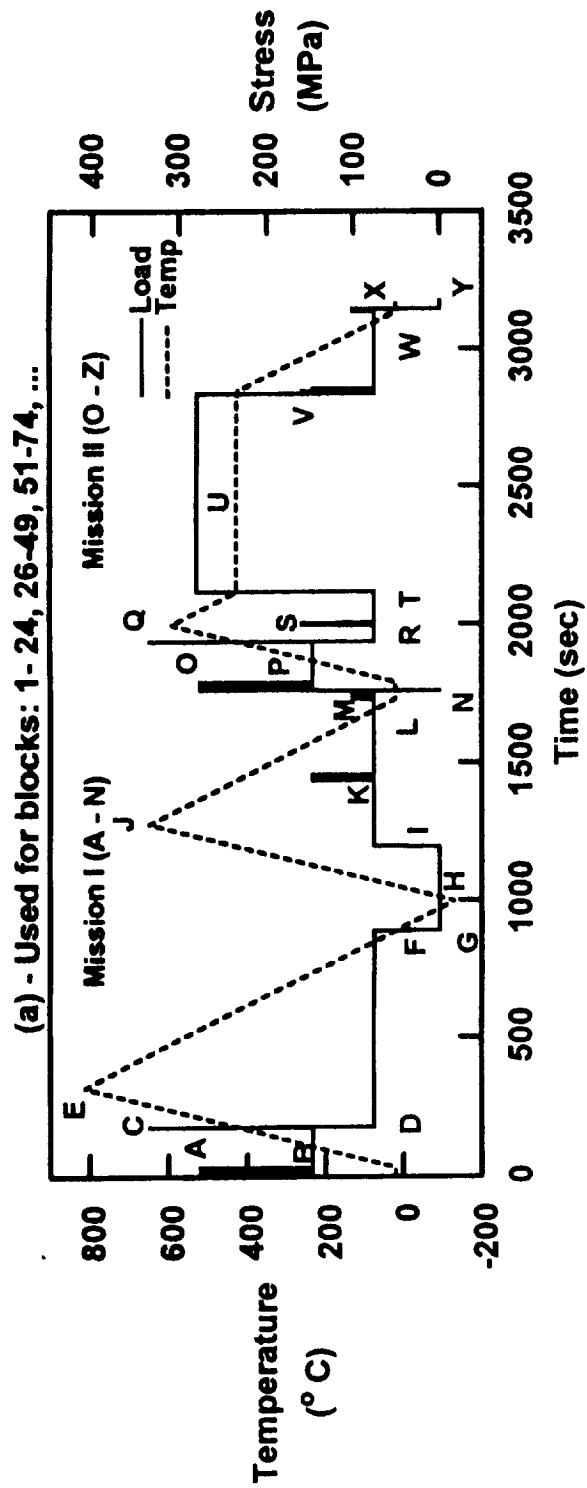
Figure 5. Generic hypersonic flight profile.

17
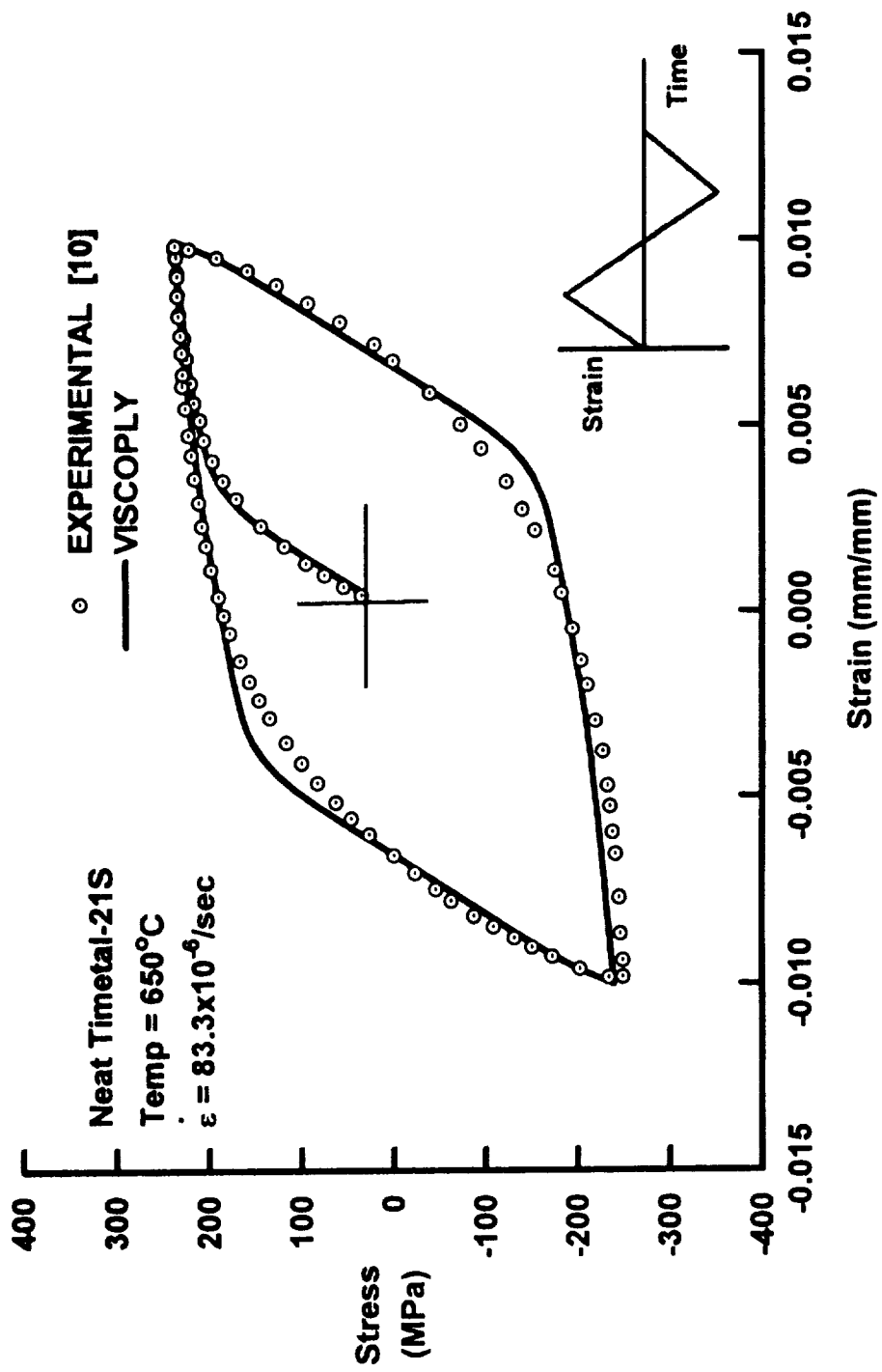
Figure 6. VISCOPLY prediction of stress-strain response of neat Timetal-21S at 650°C.

18
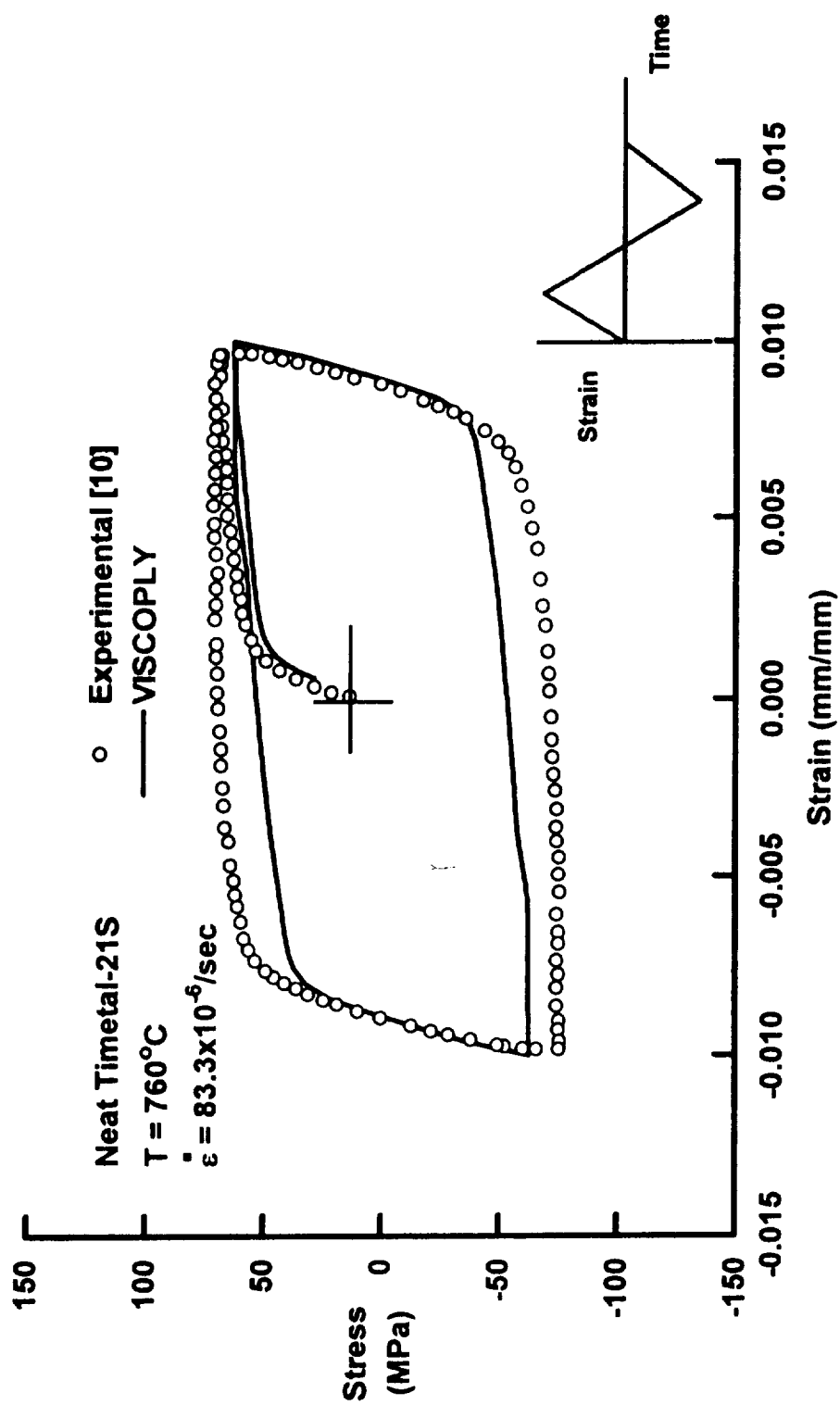
Figure 7. VISCOPLY prediction of stress-strain response of Timetal-21S at 760°C.

19
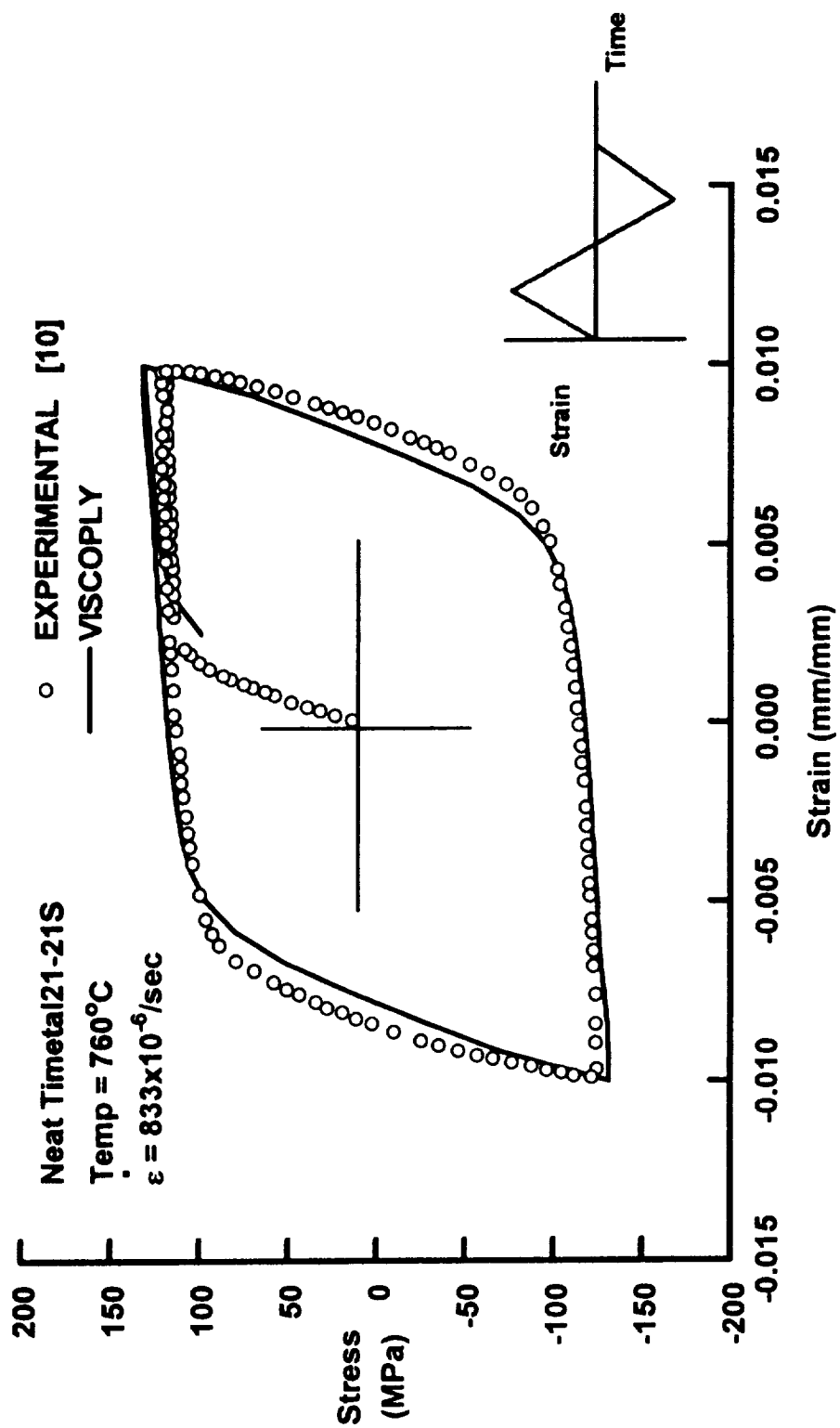
Figure 8. VISCOPLY prediction of stress-strain response of Timetal-21S at 760°C.
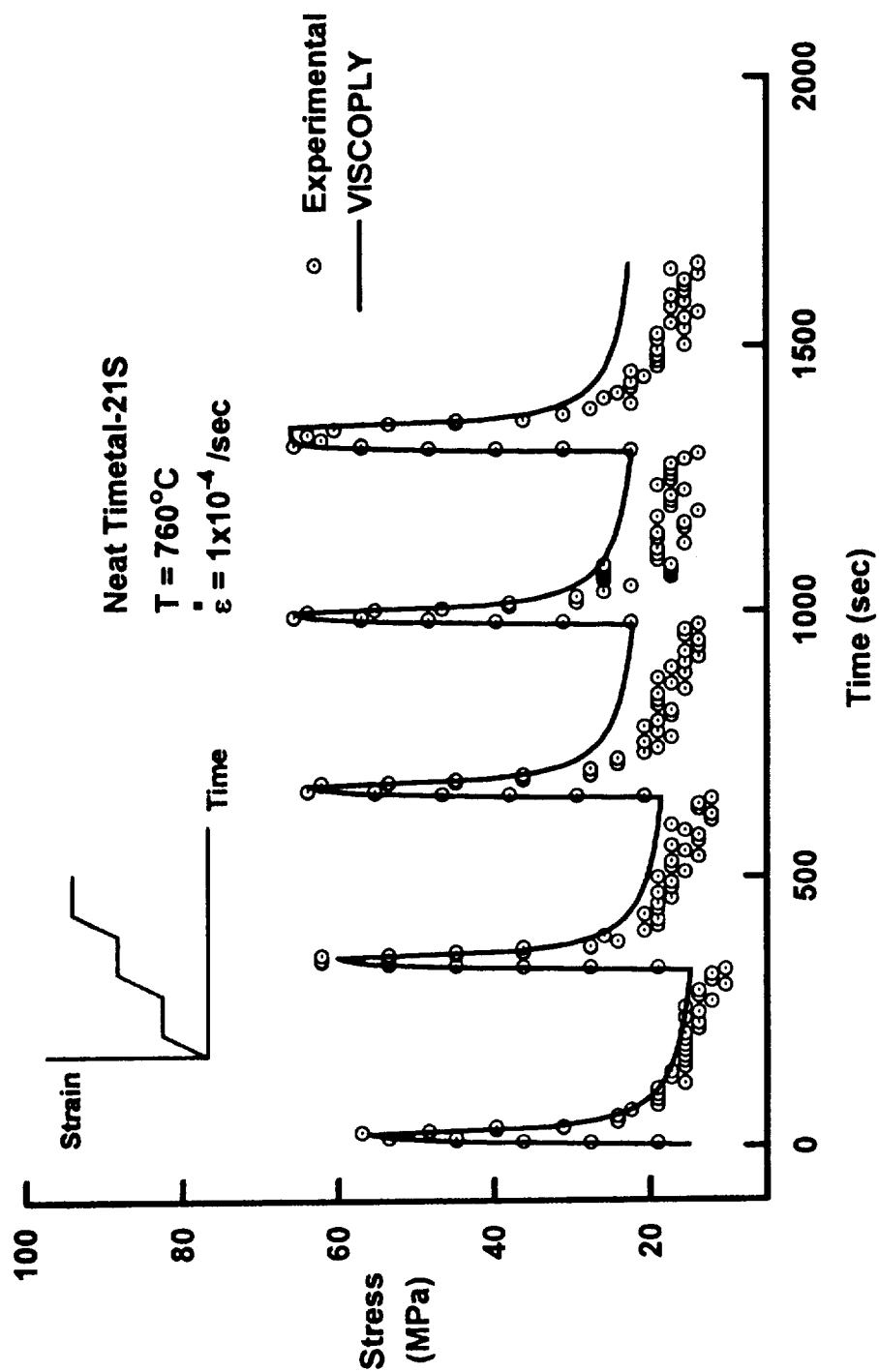
Figure 9. VISCOPLY prediction of time-dependent response of Timetal-21S at 760°C.

21
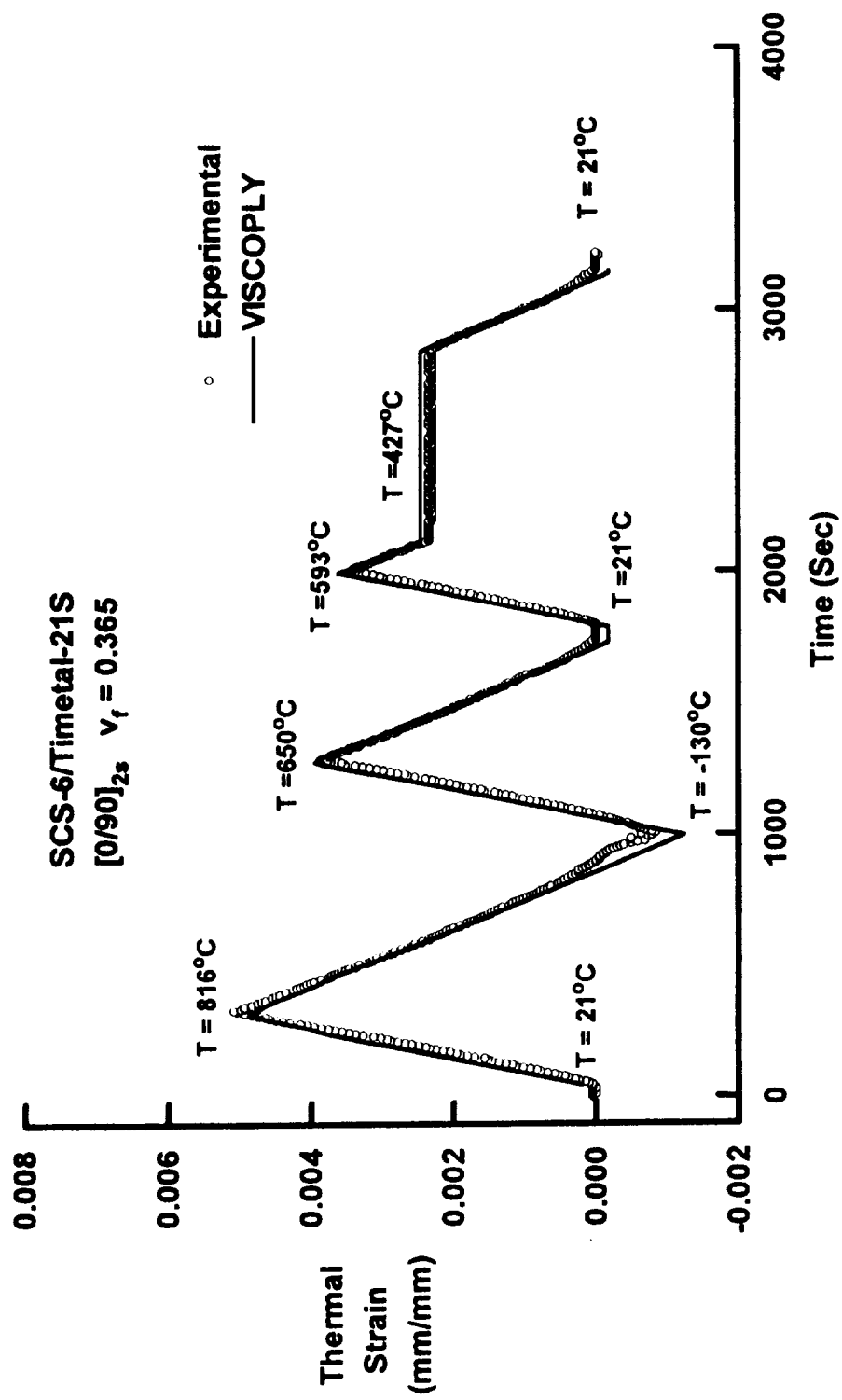
Figure 10. VISCOPLY prediction of the thermal strain as a function of time.
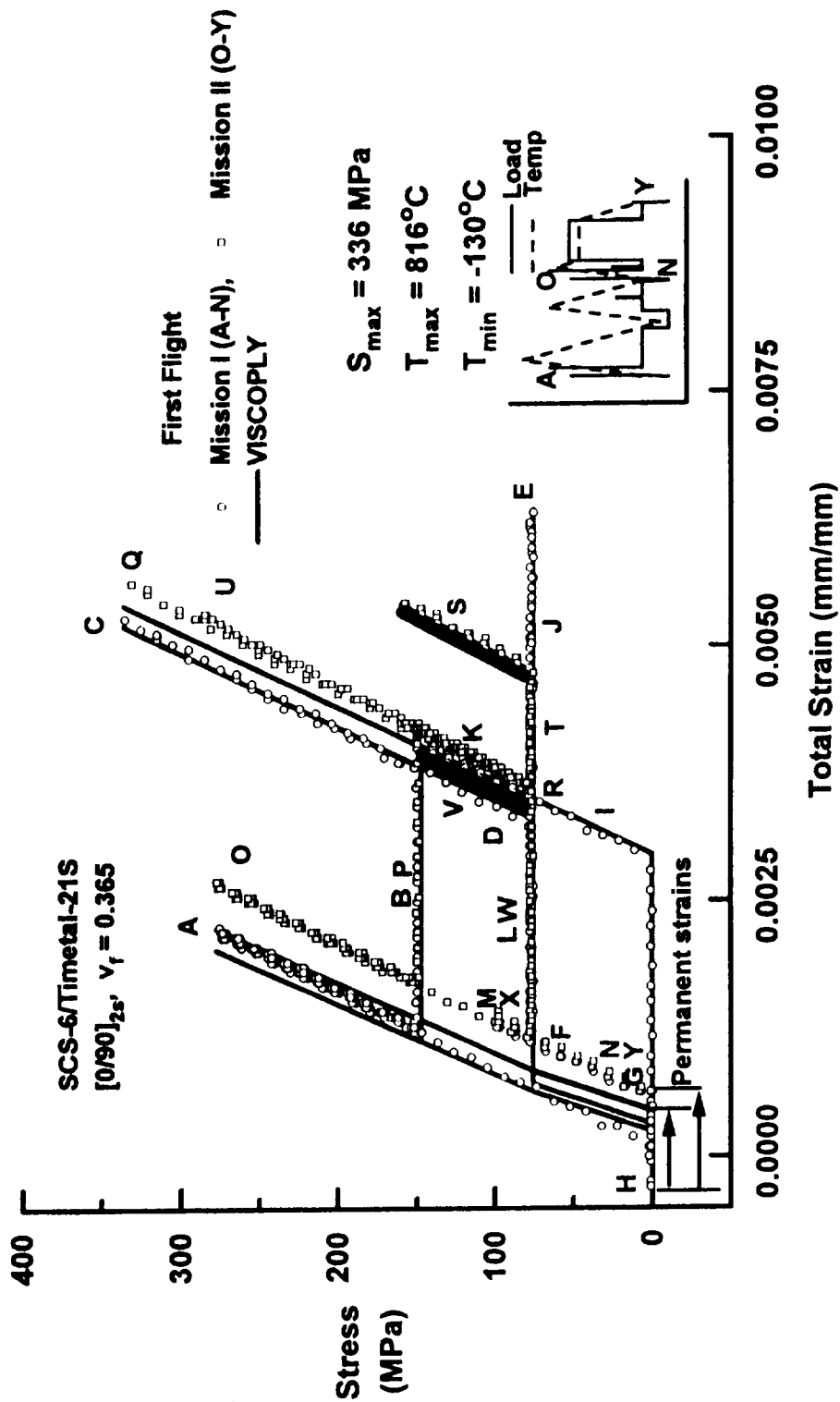
Figure 11. VISCOPLY prediction of stress-strain response during the first flight profile.
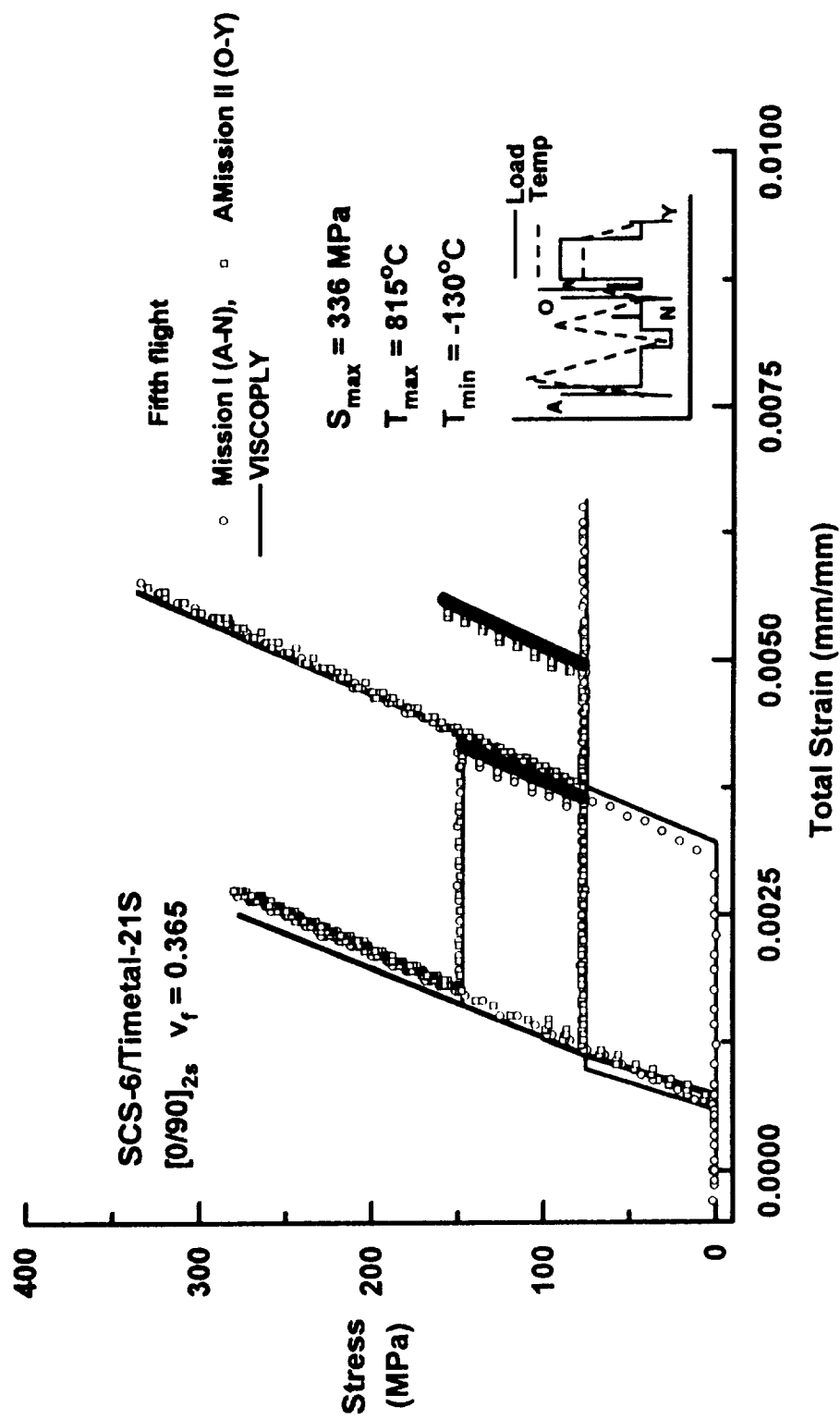
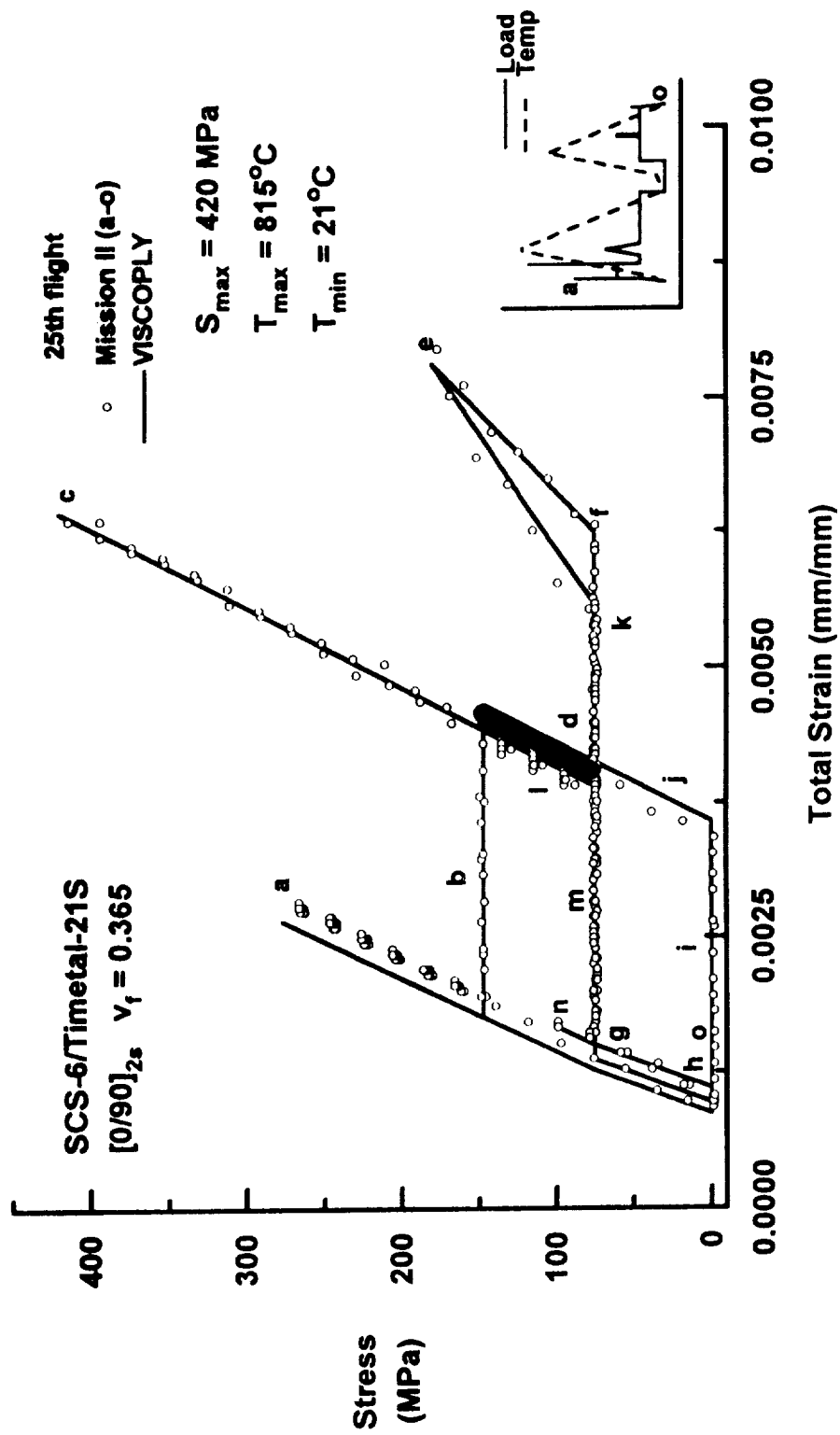Figure 12. VISCOPLY prediction of stress-strain response during the fifth flight profile.
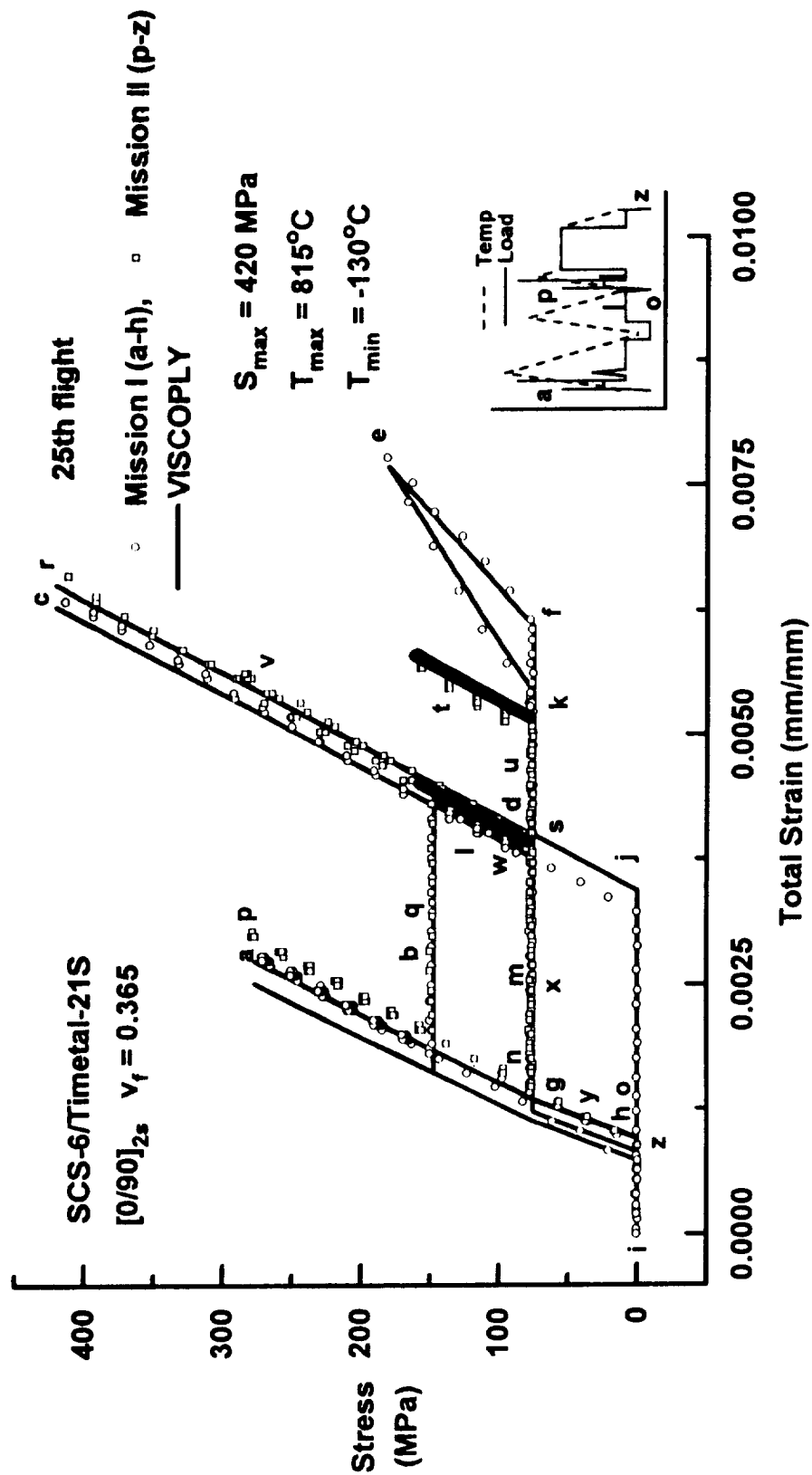
Figure 13. VISCOPLY prediction of stress-strain response during the 25th flight profile.
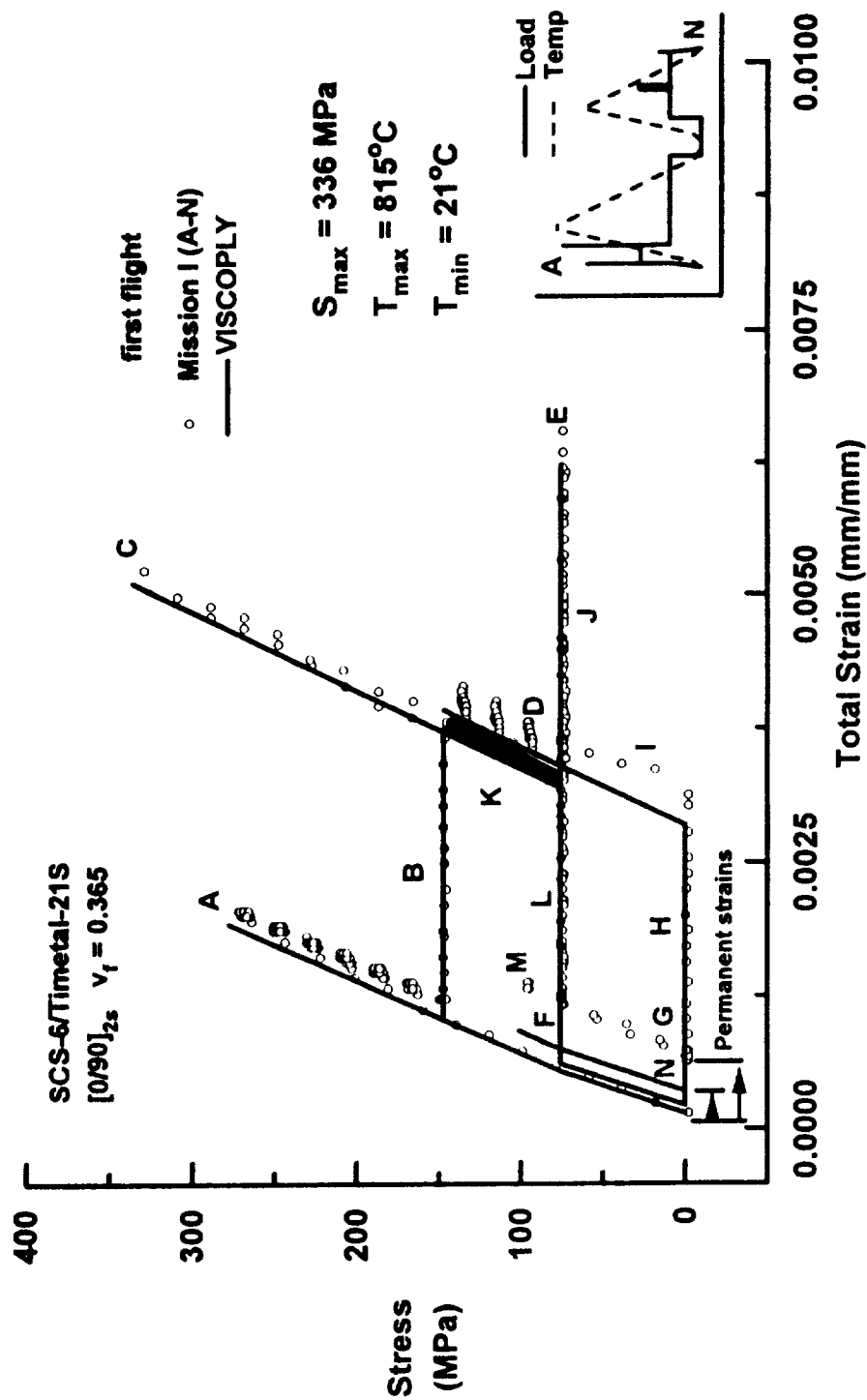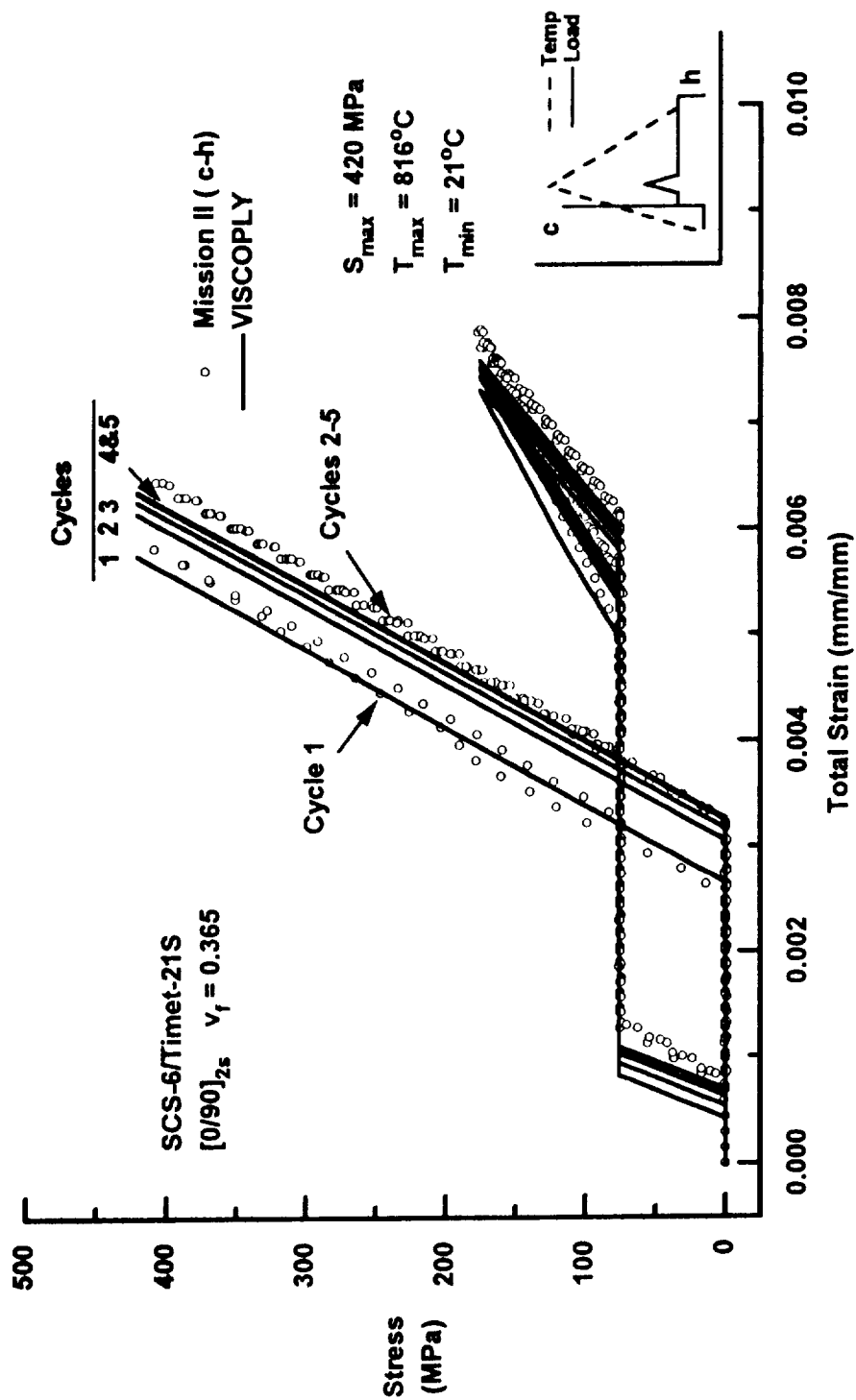
Figure 14. VISCOPLY prediction of stress-strain response during the first flight profile.

26
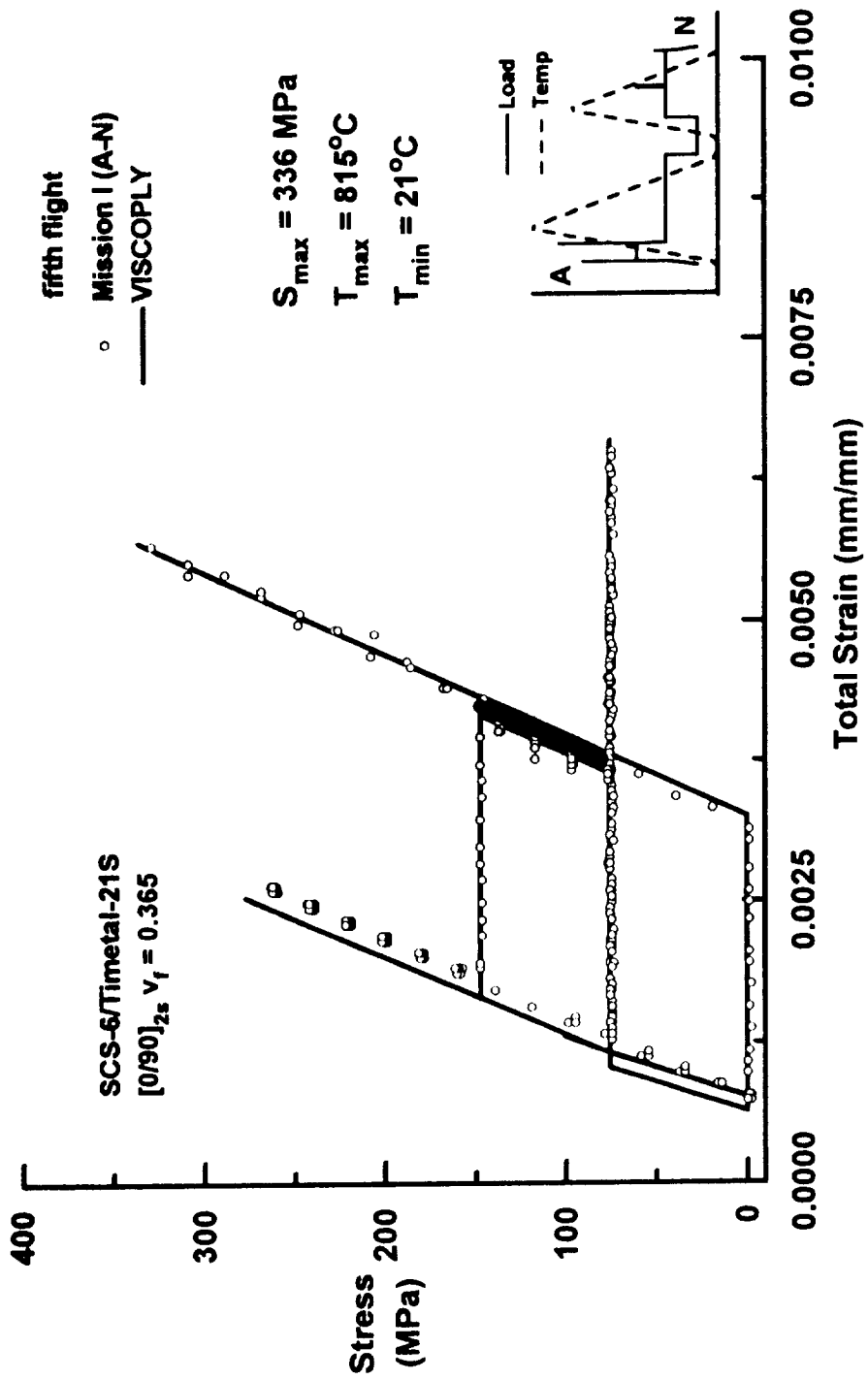
Figure 15. VISCOPLY prediction of stress-strain response during the fifth flight profile.

SCS-6/Timetal-21S
[0/90]$_{2s}$ v$_f$ = 0.365

fifth flight
o   Mission I (A-N)
—— VISCOPLY

S$_{max}$ = 336 MPa
T$_{max}$ = 815°C
T$_{min}$ = 21°C

27

Figure 16. VISCOPLY prediction of stress-strain response during the 25th flight profile.

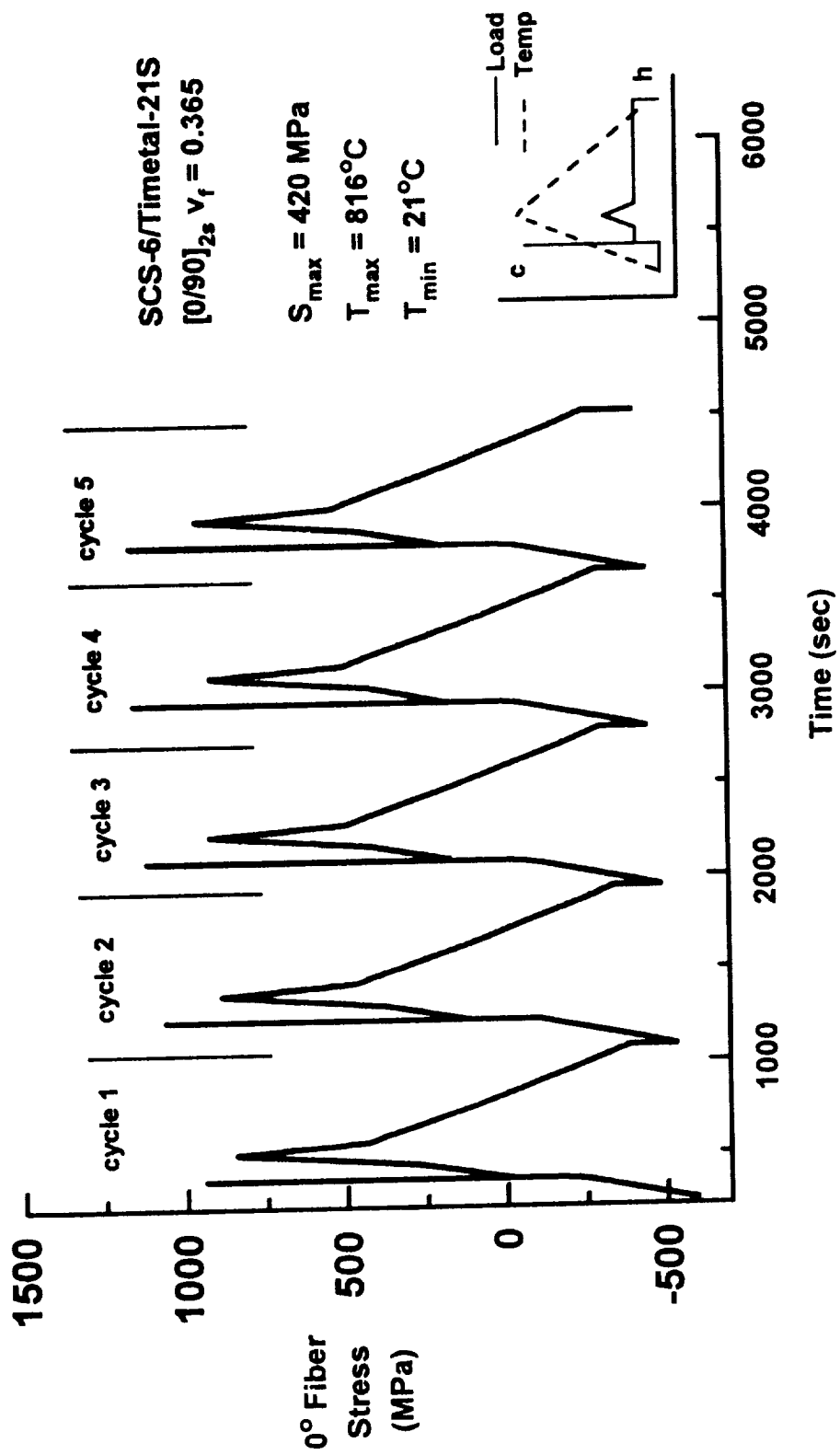Figure 17. VISCOPLY prediction of stress-strain response to a portion of flight profile.

Figure 18. VISCOPLY prediction of 0° fiber stress as a function of time.

30

REPORT DOCUMENTATION PAGE

1. AGENCY USE ONLY (Leave blank)	2. REPORT DATE February 1994	3. REPORT TYPE AND DATES COVERED Technical Memorandum

4. TITLE AND SUBTITLE

Prediction of Stress-Strain Response of SCS-6/Timetal-21S
Subjected to a Hypersonic Flight Profile

5. FUNDING NUMBERS

WU 505-63-50-04

6. AUTHOR(S)

Massoud Mirdamadi and W. Steven Johnson

7. PERFORMING ORGANIZATION NAME(S) AND ADDRESS(ES)

NASA Langley Research Center
Hampton, VA 23681-0001

8. PERFORMING ORGANIZATION REPORT NUMBER

9. SPONSORING / MONITORING AGENCY NAME(S) AND ADDRESS(ES)

National Aeronautics and Space Administration
Washington, DC 20546-0001

10. SPONSORING / MONITORING AGENCY REPORT NUMBER

NASA TM 109026

11. SUPPLEMENTARY NOTES

Mirdamadi: Analytical Services and Materials, Inc., Hampton, VA; Johnson: Langley Research Center, Hampton, VA

12a. DISTRIBUTION AVAILABILITY STATEMENT

Unclassified - Unlimited

Subject Category - 24

12b. DISTRIBUTION CODE

13. ABSTRACT (Maximum 200 words)

Thermomechanical response of a cross-ply SCS-6/Timetal-21S composite subjected to a generic hypersonic flight profile with the temperature ranging from -130°C to 816°C was evaluated experimentally and analytically. A two dimensional micromechanical analysis, VISCOPLY, was used to predict the stress-strain response of the laminate and of the constituents in each ply during thermomechanical loading conditions. In the analysis, the fiber was modeled as elastic with transverse orthotropic and temperature dependent properties and the matrix was modeled using a thermo-viscoplastic constitutive relation. The fiber transverse modulus was reduced in the analysis to simulate fiber-matrix interface failure. Reasonable agreement was found between measured and predicted laminate stress-strain response when fiber-matrix debonding was modeled.

14. SUBJECT TERMS

Silicon-carbide fibers; Residual stresses; Interface; Thermal strain;
Viscoplasticity theory

15. NUMBER OF PAGES
31

16. PRICE CODE
A03

17. SECURITY CLASSIFICATION OF REPORT Unclassified	18. SECURITY CLASSIFICATION OF THIS PAGE Unclassified	19. SECURITY CLASSIFICATION OF ABSTRACT	20. LIMITATION OF ABSTRACT